Michael Habeck*, Hafiza Nosheen Saleem, Daria Plota, Cleophas Cheruiyot, Tobias Kohl, Stephan E. Lehnart, Stefan Jakobs and Antje Ebert*

Sarcomere analysis in human cardiomyocytes by computing radial frequency spectra

https://doi.org/10.1515/hsz-2025-0173
Received July 4, 2025; accepted December 12, 2025;
published online December 29, 2025

Abstract: In cardiomyocytes, the basic contractile unit are sarcomeres, which are organized in a regular manner facilitating their function. Here, we present a new computational approach to assess the functional properties of sarcomeres at the nanoscale level in human cardiac cells, induced pluripotent stem cell-derived cardiomyocytes (iPSC-CMs). We combined our analysis to different types of high-resolution imaging data, structured illumination microscopy (SIM), stimulated emission depletion (STED) microscopy-based imaging, as well as confocal microscopy data. We show that the radially averaged magnitude spectrum (RAMS) revealed sarcomere properties in a human cardiomyocyte model, iPSC-CMs, and compared our RAMS-based analysis to a real-space approach based on manually selected regions of interest. Moreover, we found the RAMS method suitable to quantify molecular differences of sarcomeres such as present in severe cardiac diseases, such as dilated cardiomyopathy (DCM). Defects in the sarcomere organization that occur in the presence of inherited DCM mutations in sarcomere proteins were efficiently recapitulated by our analysis. This new approach may facilitate streamlined analysis of molecular disease-specific phenotypic imaging data of cardiac cells, aiding our deeper understanding of the molecular basis of cardiac diseases.

Keywords: sarcomere; human iPSCs; computational modelling; signal transduction; STED; dilated cardiomyopathy

***Corresponding authors: Michael Habeck**, University Medical Center Jena, Microscopic Image Analysis Group, Jena University Hospital, D-07743, Jena, Germany, E-mail: Michael.Habeck@med.uni-jena.de; and **Antje Ebert**, Department of Cardiology and Pneumology, Heart Research Center Göttingen, University Medical Center Göttingen, Georg-August University of Göttingen, Robert-Koch-Strasse 40, D-37075, Göttingen, Germany; DZHK (German Center for Cardiovascular Research), Partner Site Göttingen, Göttingen, Germany; and Cluster of Excellence "Multiscale Bioimaging: From Molecular Machines to Networks of Excitable Cells", University of Göttingen, Göttingen, Germany, E-mail: antje.ebert@med.uni-goettingen.de. https://orcid.org/0000-0002-3642-242X (A. Ebert)
Hafiza Nosheen Saleem, Daria Plota and Cleophas Cheruiyot, Department of Cardiology and Pneumology, Heart Research Center Göttingen, University Medical Center Göttingen, Georg-August University of Göttingen, Robert-Koch-Strasse 40, D-37075, Göttingen, Germany; and DZHK (German Center for Cardiovascular Research), Partner Site Göttingen, Göttingen, Germany
Tobias Kohl and Stephan E. Lehnart, Department of Cardiology and Pneumology, Heart Research Center Göttingen, University Medical Center Göttingen, Georg-August University of Göttingen, Robert-Koch-Strasse 40, D-37075, Göttingen, Germany; DZHK (German Center for Cardiovascular Research), Partner Site Göttingen, Göttingen, Germany; and Cluster of Excellence "Multiscale Bioimaging: From Molecular Machines to Networks of Excitable Cells", University of Göttingen, Göttingen, Germany
Stefan Jakobs, Cluster of Excellence "Multiscale Bioimaging: From Molecular Machines to Networks of Excitable Cells", University of Göttingen, Göttingen, Germany; Department of NanoBiophotonics, Research Group Mitochondrial Structure and Dynamics, Max Planck Institute for Multidisciplinary Sciences, Göttingen, Germany; Clinic of Neurology, High Resolution Microscopy, University Medical Center Göttingen, Göttingen, Germany; and Fraunhofer Institute for Translational Medicine and Pharmacology ITMP, Translational Neuroinflammation and Automated Microscopy, Göttingen, Germany

1 Introduction

In cardiomyocytes, excitable contractile cells, the smallest contractile unit are the sarcomeres, which generate contractile force in a Ca^{2+}-dependent manner by sliding of actin-myosin filaments. Sarcomeres are organized in a highly regular manner, which is critical for their efficient function. Thus, sarcomeres properties are a basic unit of understanding the function of cardiomyocytes. This is critical as sarcomere functions are pathologically altered in a variety of cardiac diseases, including cardiomyopathies, a frequent cause of heart failure. Cardiomyopathies, such as dilated cardiomyopathy, are caused in more than 25–30 % of cases by inherited mutations, which typically occur in proteins of the sarcomeres (Eldemire et al. 2024, McNally and Mestroni 2017). Mutations in sarcomere proteins can deform protein structures within the sarcomere, resulting in sarcomere disorganization and altered contractility as well as force generation (Eschenhagen and Carrier 2019, van der Velden and Stienen 2019). Therefore, accurate quantification of sarcomere properties is a cornerstone not only to structural and computational modelling of cardiomyocyte biomechanics but is vital to molecular studies of human cardiac pathologies. Previous methods of sarcomere analysis

Open Access. © 2025 the author(s), published by De Gruyter. This work is licensed under the Creative Commons Attribution 4.0 International License.

typically considered individual imaging strategies (Chopra et al. 2018, Douglas et al. 2024, Hinson et al. 2015). We present here an alternative method for analysis of sarcomere features with multiple imaging technologies and demonstrate its applicability for assessment of disease-specific dysfunctions in sarcomeres. We used a state-of-the-art human cardiac cell model of induced pluripotent stem cell-derived cardiomyocytes (iPSC-CMs). While human iPSC-CMs represent an early stage of heart development (Ebert et al. 2015, Eschenhagen and Carrier 2019), they are functional human cardiac cells that can be cultured *in vitro* and enable to study pathological sarcomere dysfunction in cardiac diseases, such as hypertrophic cardiomyopathy (Lan et al. 2013) and dilated cardiomyopathy (DCM) (Sun et al. 2012).

We employed iPSC-CMs carrying an inherited DCM mutation in a sarcomere protein critical for contractility, tropomyosin (TPM1)-L185F, described earlier (Dai et al. 2023, Saleem et al. 2024). The DCM iPSCs were generated by introducing the DCM mutation, TPM1-L185F, into WT iPSCs using CRISPR/Cas9 genome editing, as reported earlier (Dai et al. 2023, Saleem et al. 2024) and are referred to as DCM mutation-introduced (Mut-int). Moreover, we employed DCM patient-specific iPSC-CMs from a patient who carried the inherited DCM mutation, TPM1-L185F, and who is a member of the same family as the WT control. The respective DCM (patient-specific) iPSC and iPSC-CMs were generated and reported earlier (Dai et al. 2023). The respective DCM iPSC-CMs were reported to display disrupted sarcomere organization, impaired contractility, and reduced force generation, same as other DCM iPSC-CMs carrying different sarcomere protein mutations (Dai et al. 2020, 2023, Hinson et al. 2015, Malkovskiy et al. 2021). Using immunohistochemistry of cardiac markers and confocal-based image analysis, we quantified distinct sarcomere characteristics in DCM iPSC-CMs, compared to WT controls. The new radially averaged magnitude spectrum (RAMS) approach presented here quantifies distances between consecutive z-discs linking adjacent sarcomeres by applying a Fourier-based analysis to establish sarcomere length and sarcomere organization.

We confirmed that the RAMS method is applicable to a wider range of state-of-the-art imaging technologies, such as structured illumination microscopy (SIM) and stimulated emission depletion (STED) microscopy-based imaging. Moreover, we corroborated sarcomere analysis with the RAMS method in 3D image layers and compared RAMS to an analysis approach reported earlier. These aspects will enable capturing nanoscale details and facilitate applicability of our approach toward its use with other types of imaging data in the future. Therefore, our findings will assist in gaining deeper insight into the molecular basis associated with DCM in cardiac cells.

2 Results

2.1 Computational simulation and fourier-based analysis of signal intensities

Sarcomeres are defined as the interval or space between two z-discs, to which the actin-based thin filaments attach. Based on this, we applied a new approach to functional analysis of sarcomeres. The z-disc pattern, detected by z-disc-specific proteins such as sarcomeric α-actinin, can be considered to correspond to a "wave" that traverses the sarcomere in longitudinal direction. The sarcomere length corresponds to the respective wavelength. Therefore, we applied Fast Fourier transform (FFT) to characterize the wave pattern formed by z-discs without requiring manual processing such as the selection of an ROI or linear segments. We first tested this approach using computational simulation of striated patterns propagating along the x-axis (Figure 1A, left) and calculated the respective magnitude spectrum by a 2D FFT (Figure 1A, right). In this idealized simulation, the frequency of the striated pattern was ten, thus the intervals were separated by a distance of 1,024/10 = 102.4 pixels. In the Fourier domain, this resulted in distinct peaks at a frequency of $k_x = \pm 10$ indicated by red dashed lines (Figure 1A, right). To determine the separating distance, the simulated image intensities (Figure 1A) were projected onto a line (the x axis in this example) (Figure 1B). The resulting profile displayed a series of peaks that are separated by a constant distance corresponding to the sarcomere length. The peaks were automatically detected with Otsu thresholding and connected-component labeling (along the x axis). The numerical values were extracted via the estimated peak locations (Figure 1B, red dashed lines) and matched the values based on Fourier analysis (Figure 1B). The Fourier approach resulted in an estimated distance of 102.40 pixels, whereas the real-space approach yielded an average value of 102.39 pixels.

In reality, the myofibrils of cardiomyocytes and thus, the striated pattern of sarcomeres can be oriented in many different directions. Therefore, we analyzed the consequences of rotated striation. For example, sarcomeres propagating in vertical direction will have the same Fourier spectrum as shown in Figure 1A but will be rotated by 90°. Employing computational simulation, we generated striated patterns rotated at an angle of 60° (Figure 1C, left), compared to Figure 1A. Consequently, in the idealized simulation, the respective Fourier spectrum was rotated by the same angle corresponding to its striated pattern (Figure 1C, right).

Sarcomeres present yet differently in early postnatal cardiomyocytes. In this developmentally early stage, immature

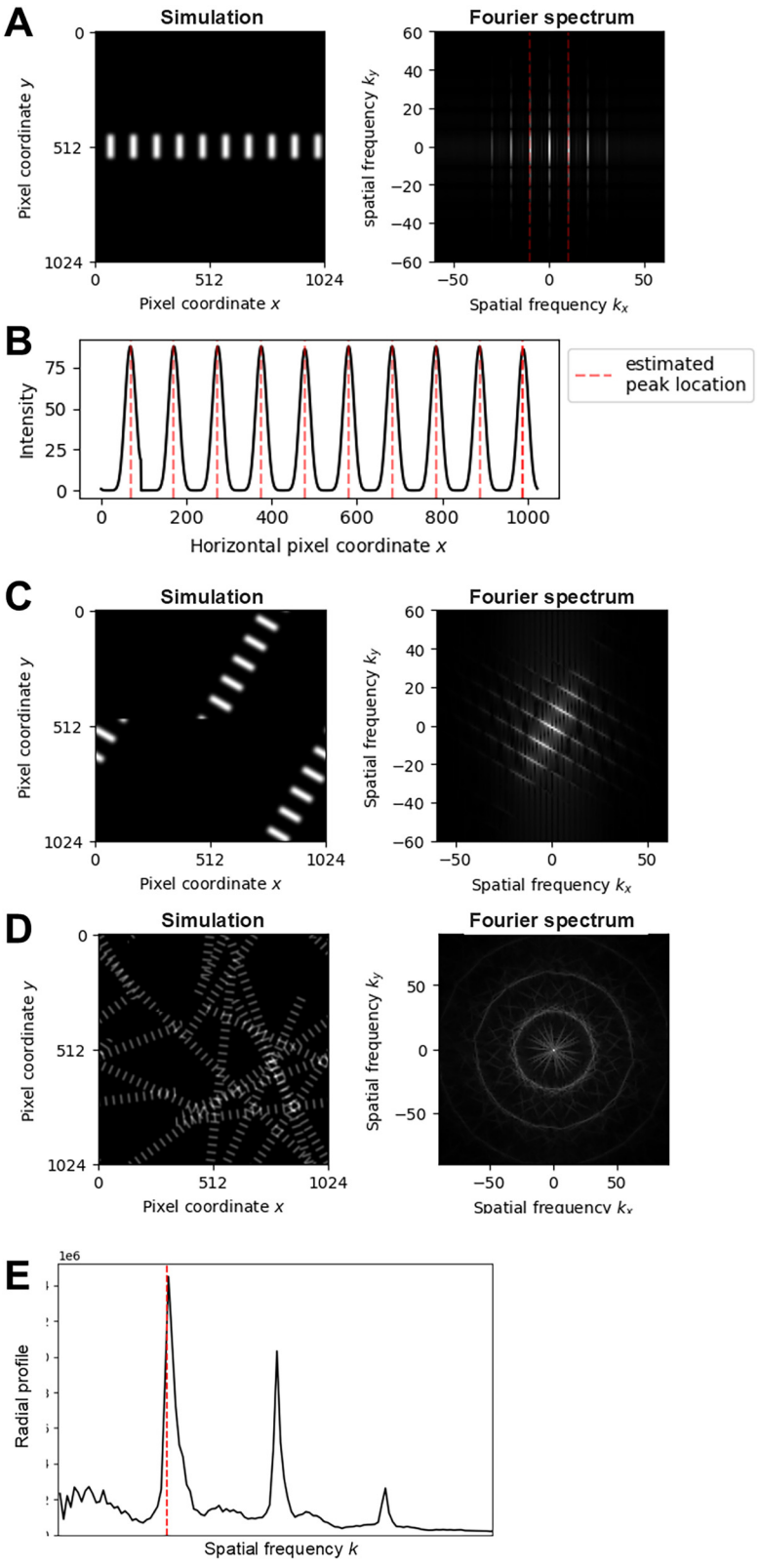


Figure 1: Computational simulation establishes peak maxima extraction via RAMS. (A) Left, computational simulation of striated patterns; (A) right, magnitude of the 2D fourier spectrum corresponding to panel (A) left. Red dashed lines indicate peaks at a frequency of $k_x = \pm 10$, based on the simulation in panel (A) and corresponding spatial frequencies along the direction of the propagating wave in frequency space. (B) Projection of the simulated image intensities to a one-dimensional profile (x axis). Automatically estimated peak locations based on otsu thresholding are marked by red dashed lines. (C) Left, computational simulation of striated patterns rotated at an angle of 60°; (C) right, 2D magnitude spectrum corresponding to panel (C) left. (D) Left, computational simulation of striated patterns oriented in different spatial directions; (D) right, magnitude spectrum corresponding to panel (D) left. (E) radially averaged magnitude spectrum (RAMS); red dashed line indicates the global maximum of the RAMS.

sarcomeres are oriented in various directions, resulting in a superposition of their Fourier spectra. Assuming isotropic orientation of striated sarcomere patterns in all spatial directions, the Fourier peaks will form a ring around the zero-frequency peak. Thus, we expected to see ring-like structures in the Fourier spectrum of sarcomeres with different orientations

as demonstrated by computational simulation (Figure 1D). The radius of the ring corresponded to the dominant frequency or, respectively, the dominant wavelength in the image.

2.2 Computing radial frequency spectra enables extraction of peak maxima

To determine the dominant frequency of striated patterns, we radially averaged the Fourier spectrum. The radially average magnitude spectrum (RAMS) enabled us to estimate the sarcomere length by locating the dominant peak. If I denoted the microscopy image and $\hat{I}$ its 2D Fourier transform with the zero-frequency component shifted to the center, the RAMS is defined as:

$$p(k) = \sum_{k_x,k_y} \left|\hat{I}(k_x,k_y)\right| \Delta\left(k - \sqrt{k_x^2 + k_y^2}\right)$$

In the definition of the radial profile p, the sum runs over all spatial frequencies and the binning function Δ is a rectangular function whose support is determined by a user-defined bin size δ:

That is, the radial profile p was $\Delta(k) = \begin{cases} 1 & \text{if } |k| \le \delta/2 \\ 0 & \text{if } |k| > \delta/2 \end{cases}$

computed by summing up all amplitudes along rings of width δ (Figure 1D). Note that in our definition of the radial profile, we omitted normalization by the number of pixels contributing to a ring at frequency k, which in two dimensions is proportional to k. The first maximum of the radial profile was located at a frequency close to the true frequency of the striated patterns (Figure 1E). With this approach, we estimated the frequency of the striated pattern to be 30.5, which is close to the true value of 30 used in the simulation.

From the estimated frequency $k_{\max}$, we obtain an estimate d of the distance between individual striations:

$$d = N / k_{\max}$$

where N is the number of pixels. For the simulated pattern, we obtained a distance estimate of 33.57 pixel (the true value is 34.13 pixels).

2.3 Analysis of high-resolution sarcomere imaging of human cardiac tissues by RAMS

Next, we sought to apply the RAMS approach to sarcomere imaging data from human cardiomyocytes. For image analysis of sarcomeres, data generated and reported earlier from human heart tissues from donor hearts rejected for transplantation (Dai et al. 2023) were employed. Following slicing, mounting, fixation and immunostaining for typical cardiac sarcomere markers, cardiac troponin T (TNNT2, TnT, Uniprot: troponin T) and sarcomeric α-actinin (ACTN2, SAA, Uniprot. alpha-actinin-2), confocal imaging was performed as reported earlier (Dai et al. 2023) (Figure 2A). Signals derived from the sarcomere contractile protein, TnT (TNNT2), as well as the z-disc-localized protein SAA (ACTN2), visualized the sarcomeres. As before for computational simulation of striated patterns (Figure 1C), in the sarcomere z-disc patterns detected via SAA (ACTN2) (Figure 2B, left), a regular wave could be considered to traverse the image plane from the lower right to the upper left corner.

As observed for computational simulation (Figure 1C), the Fourier spectrum showed marked peaks close to the central zero-frequency maxima that were oriented longitudinally with the sarcomeres (Figure 2B, right). Because the sarcomere filaments in the CMs of adult human heart tissue are aligned in parallel, no ring structure emerged in the magnitude spectrum (Figure 2B, right). Based on the Fourier spectrum, the RAMS was obtained (Figure 2C). Radial frequency spectra analysis enabled locating the dominant frequency. Accordingly, RAMS allowed us to derive an estimate of the sarcomere length of 1.73 µm.

2.4 Application of RAMS analysis to DCM iPSC-CMs

For experimental and translational research, human CMs from adult heart tissues are a most suitable model, however, are difficult to obtain and cannot be cultured nor modified *in vitro* (Zhao et al. 2020). In this context, human iPSC-CMs, which represent an early post-natal stage of human CMs (Ebert et al. 2015, Eschenhagen and Carrier 2019), are an alternative model for research purposes. Therefore, human iPSC-CMs were employed to test the RAMS approach for image analysis of sarcomeres. Human iPSC-CMs were derived using previously described protocols (Dai et al. 2023) from the iPSCs of healthy controls (WT) or isogenic, CRISPR/Cas mutation-introduced DCM iPSCs carrying the inherited DCM mutation TPM1-L185F, both of which were reported earlier (Dai et al. 2023). Human iPSC-CMs derived from these lines and respective protocols were characterized and reported before (Dai et al. 2023). Both WT and DCM (mut-int) iPSC-CMs expressed typical cardiac sarcomere markers, including cardiac troponin T (TNNT2, TnT, Uniprot: troponin T) as well as sarcomeric α-actinin (ACTN2, SAA, Uniprot. alpha-actinin-2) (Figure 3A). Human WT and DCM (mut-int) iPSC-CMs were fixed, permeabilized, and subjected to

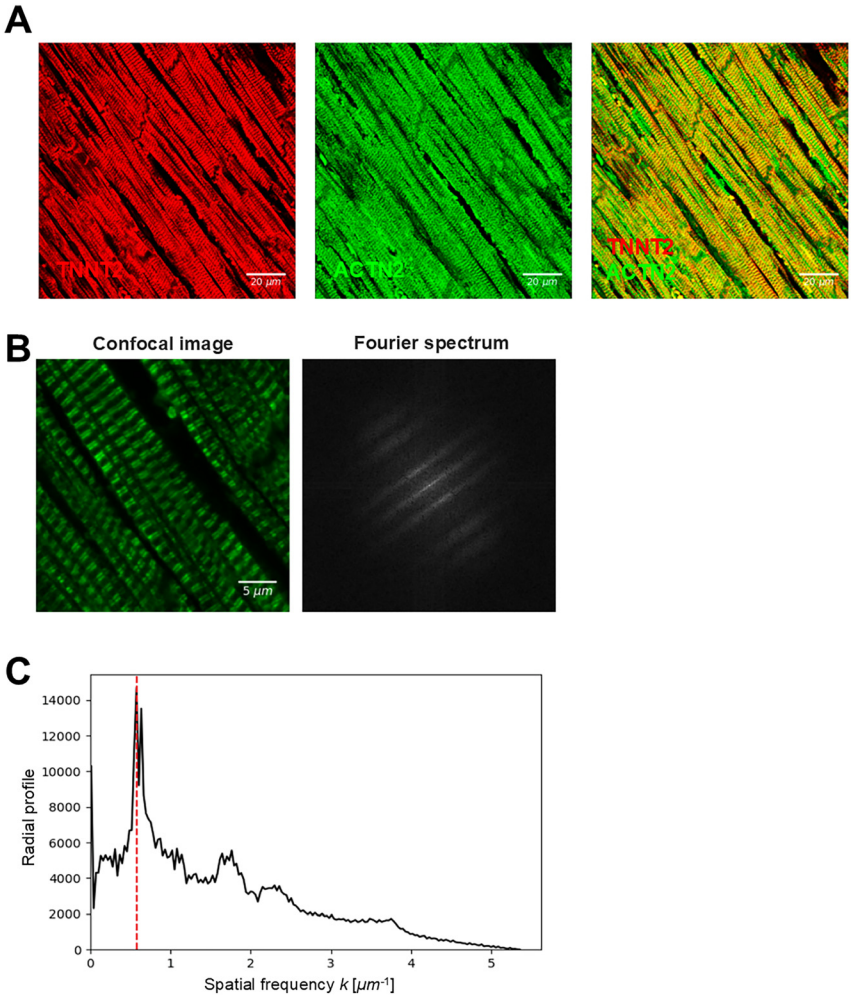


Figure 2: RAMS-based analysis of high-resolution sarcomere imaging of human cardiac tissues. (A) Human heart tissue section following immunostaining with antibodies against cardiac troponin T (TNNT2, TnT, uniprot: Troponin T), sarcomeric α-actinin (ACTN2, SAA, uniprot. Alpha-actinin-2). A representative image from an earlier report (Dai et al. 2023) is shown. (B) Left, zoomed-in region of the confocal image shown in the middle panel of (A), revealing sarcomere z-discs detected by sarcomeric α-actinin (SAA, ACTN2, uniprot. Alpha-actinin-2); (B) right, magnitude spectrum obtained with a 2D fourier transform of the selected region. (C) Radially averaged magnitude spectrum showing peaks at distinct frequencies in fourier space, based on which the corresponding sarcomere length is computed (red highlighted).

immunostaining via specific antibodies reported earlier (Dai et al. 2020). High-resolution confocal imaging demonstrated striated patterns of WT control or DCM (mut-int) iPSC-CMs (Figure 3A and B). The confocal image of human WT shown in Figure 3A exhibits striated patterns propagating in multiple spatial directions. As predicted by simulation, the magnitude spectrum shows a strong ring-like pattern (Figure 3C). To determine the radius of the ring, we computed the RAMS by radially averaging the magnitude spectrum, which resulted in a one-dimensional profile with prominent peaks at certain frequencies (Figure 3D). Based on the location of the first peak, the sarcomere length was estimated to be 1.81 µm in WT iPSC-CMs.

Next, we applied the RAMS-based analysis also to high-resolution images of DCM (mut-int) iPSC-CMs (Figure 3B). Again, a ring pattern emerged in the Fourier domain (Figure 3E) albeit weaker than for WT iPSC-CMs suggesting the sarcomere structure is less well organized in DCM (mut-int) iPSC-CMs. Using the RAMS (Figure 3F) the sarcomere length was found to be reduced, in line with our previous publication of the respective image data set (Dai et al. 2023). The sarcomere length was estimated to be 1.60 µm for DCM (mut-int) iPSC-CMs. Due to the inherited mutation of a contractile protein, TPM1, the DCM (mut-int) iPSC-CMs displayed a lower degree of organization, which was reflected in the diffuse ring pattern and wider peak ranges of the respective radial profile (Figure 3F). For a better comparison, the radial profiles of both WT iPSC-CM and DCM (mut-int) iPSC-CMs are shown side-by-side (Supplementary Figure 2). The differences in the sarcomere lengths become visible via the different locations of the first peak. The lower degree of structural organization in DCM (mut-int) iPSC-CM is reflected in a decrease of the peak amplitude and a broadening of the peaks. Thus, the RAMS-based approach enables not only analysis of the sarcomere length but also the regularity of the sarcomere arrangement as an additional parameter, which may be altered in DCM (mut-int) iPSC-CM models. To demonstrate this, the radial profiles for simulated striated

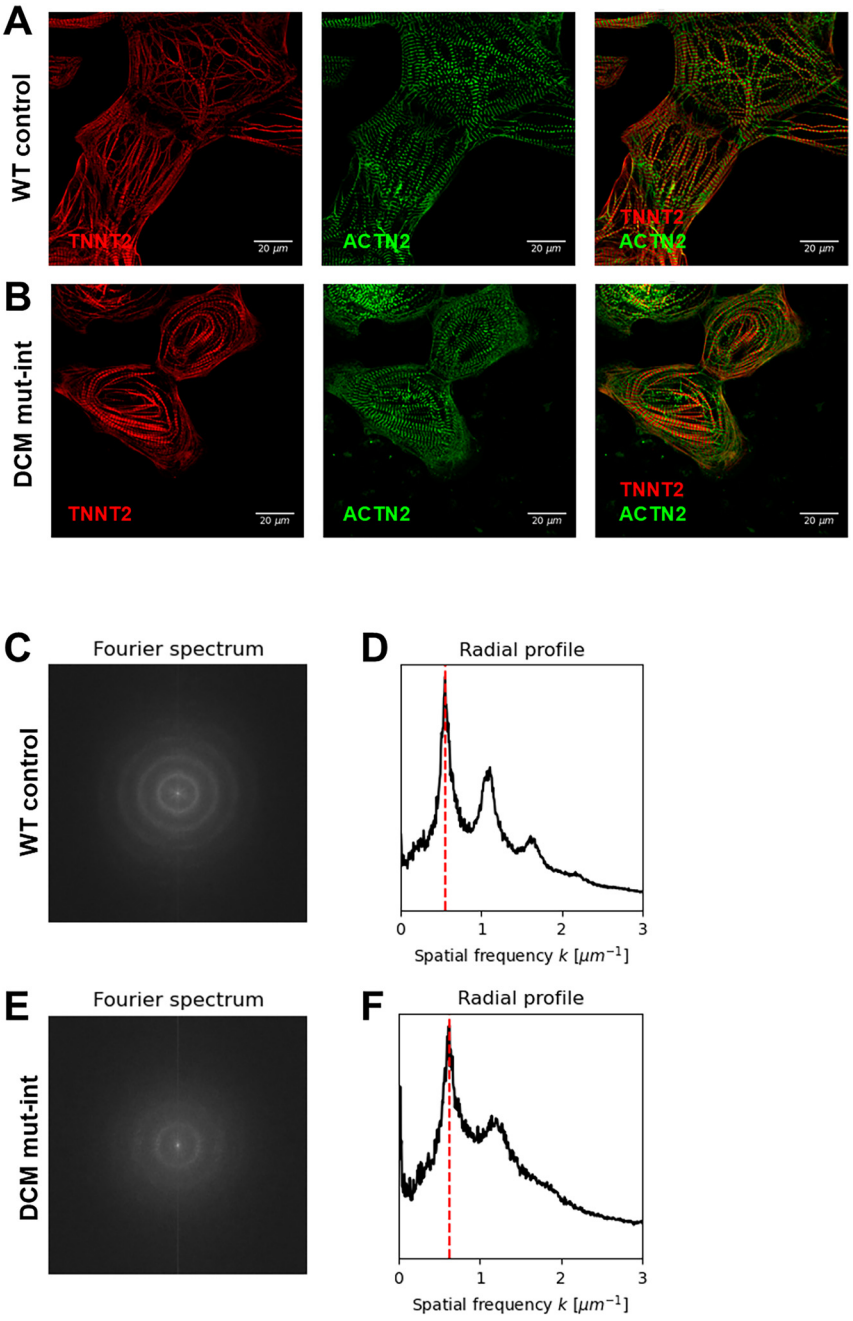


Figure 3: Application of RAMS analysis to sarcomere images from human DCM iPSC-CMs. (A, B) representative confocal images of immunostaining for two well-established sarcomere protein markers, cardiac troponin T (TNNT2, TnT, uniprot: Troponin T), and sarcomeric alpha-actinin sarcomeric α-actinin (SAA, ACTN2, uniprot: Alpha-actinin-2) in WT (control) iPSC-CMs (A) compared to DCM (CRISPR/Cas mutation-introduced, DCM mut-int) iPSC-CMs carrying a disease-causing mutation in tropomyosin, TPM1-L185F (B). The images are part of an earlier report (Dai et al. 2023). (C, F) magnitude spectra obtained with a 2D fourier transform of the images shown in panels (A) and (B), respectively. (D, G) radial profiles for the fourier spectra shown in panels (C) and (F); red dashed line indicates the dominant frequency for the respective images. (A), (C), (D), WT (control) iPSC-CMs; (B), (E), (G), DCM (mut-int) iPSC-CMs. In total, WT, 1.77 ± 0.07 µm (10 different images); DCM (mut-int), 1.51 ± 0.08 µm (8 different images). Data are shown as mean±ST DEV.

patterns are shown for a fixed peak distance (Supplementary Figure 3A) and a perturbed peak distance (Supplementary Figure 3B).

2.5 Comparison of RAMS to segmentation-based signal processing from imaging data

To validate our approach, we compared RAMS-based sarcomere analysis to a different method previously reported (Dai et al. 2020, Malkovskiy et al. 2021, Xu et al. 2021). To establish sarcomere properties, the reference method applied analysis based on region of interests (ROIs). As successive z-disc separate and link adjacent sarcomeres, measuring the distance between two successive z-lines allowed us to estimate the length of the sarcomere with its border marked by the two z-discs. To estimate the length of sarcomeres using high-resolution confocal microscopy images of iPSC-CMs (WT control) (Figure 4A), we utilized intensity projections along each linear segment and thereby obtained a one-dimensional curve that exhibits local maxima (Figure 4B). Following

application of Otsu thresholding, the distances between successive peaks were computed and enabled us to estimate the sarcomere length (Figure 4C and D). Using all ROIs, we obtained 81 estimates of the sarcomere length in WT iPSC-CMs with a mean and standard deviation of 1.84 ± 0.14 µm for the representative image shown (Figure 4). In comparison, the RAMS-based method delivered a value (1.81 µm) in good agreement with the ROI-based analysis.

When applying the same procedure to confocal images of DCM (mut-int) iPSC-CMs, we obtained results (Figure 4E–H) in line with the above findings. From all ROIs, we obtained 32 measurements of the sarcomere length with a mean value and standard deviation of 1.59 ± 0.20 µm. Again, the value obtained with the RAMS analysis (1.60 µm) for the representative image shown (Figure 4) was in good agreement with the ROI-based analysis.

2.6 Application of RAMS to imaging data from different high-resolution microscopy techniques

We next explored whether the RAMS-based analysis would be qualified to analyze sarcomere parameters of other high-resolution imaging technologies. We selected Structured Illumination Microscopy (SIM) (Figure 5A) as well as Stimulated Emission Depletion (STED) microscopy images of DCM (patient-specific) iPSC-CMs (Figure 5B, Supplementary Figure 1). Application of spectral analysis to SIM (Figure 5C) and STED (Figure 5F, Supplementary Figure 1) data enabled us to compute magnitude spectra via 2D FFT (Figure 5D–G), based on which we computed radially averaged frequency spectra (Figure 5E–H) and derived the sarcomere length. The estimated sarcomere length for the SIM image was 1.58 µm. Analysis of the STED image gave a slightly deviant value of 1.66 µm, likely due to the different modalities of the respective different imaging technique.

Together, the RAMS-based method enabled us to analyze sarcomere properties such as sarcomere length and organization in high-resolution imaging data derived from human DCM iPSC-CMs as well as controls. Moreover, RAMS analysis can be applied to data obtained via different high-resolution imaging techniques.

3 Discussion

Sarcomeres are the basic units generating contractile force in striated muscle. Their regularity is crucial for regular function of muscle cells and is altered in severe cardiac diseases such as cardiomyopathy and heart failure (Eschenhagen and Carrier 2019, van der Velden and Stienen 2019). Several previous reports presented strategies for sarcomere measurements, which retrieved the sarcomere length as a measure of z-disc distances and by defining a point of reference followed by Fast Fourier transform (Chopra et al. 2018, Douglas et al. 2024, Hinson et al. 2015). Moreover, based on manual selection, intensity profiles and feature extraction were combined to conveniently extract multiple as well as individual sarcomere intervals (Baheux Blin et al. 2024). Other studies focused on live cell analysis via movie recording and employed image segmentation to derive parameters corresponding to the entire visualized population of sarcomeres (Zhao et al. 2021) including computation of wavelet peaks (Toepfer et al. 2019). In contrast, the radially average magnitude spectrum (RAMS) approach characterizes functional sarcomere properties such as sarcomere length and organization in an automated manner using entire images without the need for manual selection. In addition, radial averaging provides not only the mean sarcomere length of the respective imaging data, but also a profile of Fourier space frequencies thereby offering insights into the regularity of sarcomere organization. Thereby, our new method offers several parameters to characterize sarcomere properties, the sarcomere length and the regularity of sarcomere arrangement. The RAMS-based method enables us to analyze the sarcomere properties of human CMs from different sources, such as adult human cardiac tissue biopsies as well as human iPSC-CMs. Moreover, RAMS analysis can be applied to data obtained via different high-resolution imaging techniques, such as confocal and structured illumination microscopy (SIM) as well as simulated emission depletion (STED) imaging. Thus, we present a new method that allows for an analysis of cardiomyocyte sarcomeres of different source and developmental stage – iPSC-derived CMs, adult CMs – with various high-resolution imaging strategies. We also show the RAMS approach to work reliably for the characterization of sarcomere properties from human iPSC-CMs carrying an DCM inherited mutation causing severe cardiac disease.

We denoted the applicability of the RAMS approach also by validating the results compared to an earlier method for sarcomere analysis which uses manual feature selection (Dai et al. 2020). This demonstrates the scope of techniques for which the RAMS method can be employed but also its potential for analysis of different types of data derived with other imaging approaches. In the future, the scope of the RAMS method could be extended by integrating machine learning or deep learning strategies for image segmentation. Together, we consider our approach a new analysis method and starting point for further quantitative modelling of sarcomere parameters. Thus, our method could support and be applied in future studies of functional

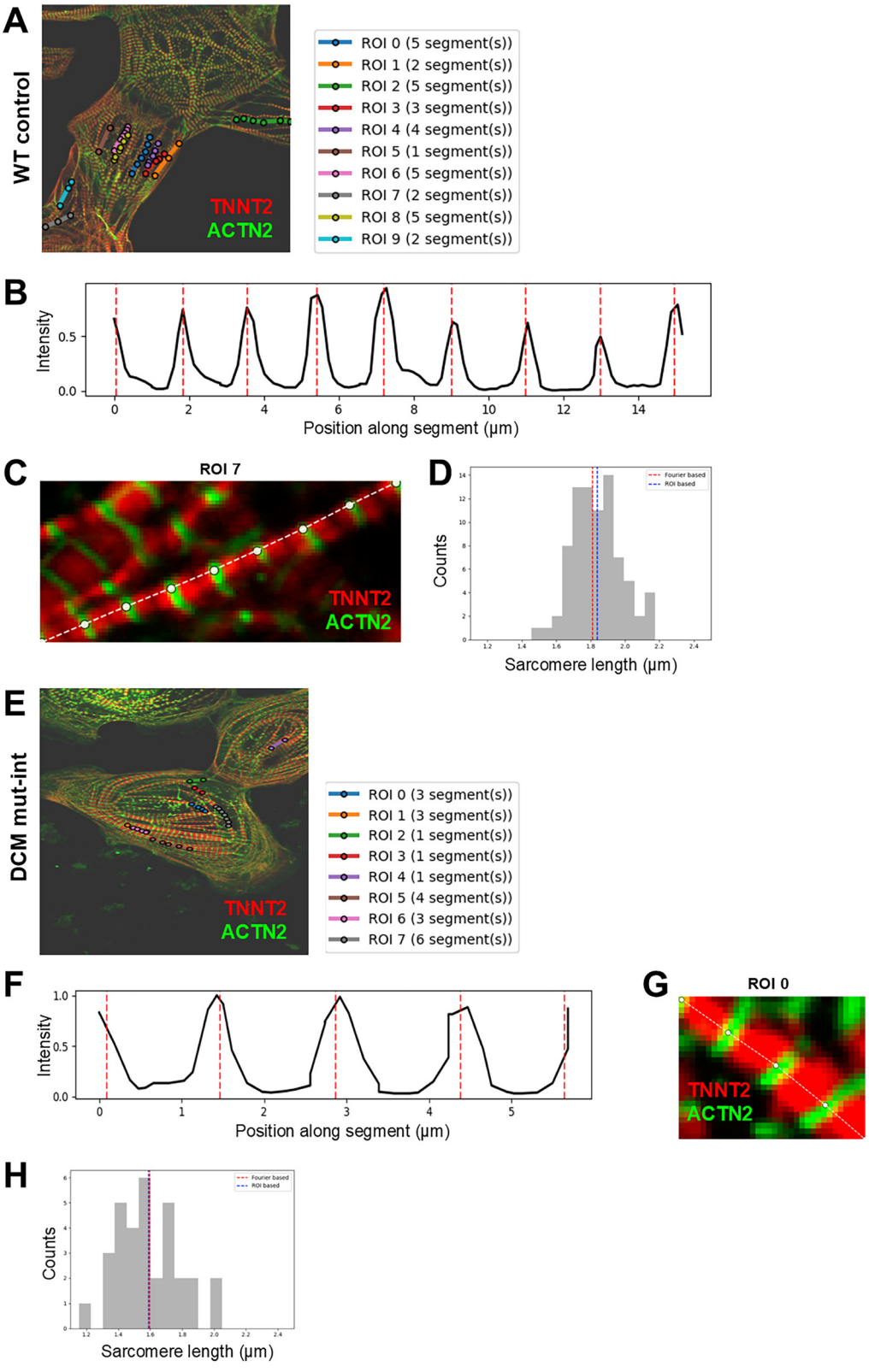


Figure 4: Comparison of RAMS to segmentation-based signal processing from imaging data to establish sarcomere properties. (A) Segmentation via regions of interest (ROIs) to collect TNNT2 (TNNT2, TnT, uniprot: Troponin T) and SAA (SAA, ACTN2, uniprot: Alpha-actinin-2)-dependent signals for WT iPSC-CM sarcomeres based on intensity projection along linear segments. A representative image, which is part of an earlier report (Dai et al. 2023), is shown. (B) One-dimensional curve exhibiting local maxima based on intensity projections. (C) Computed peak locations after otsu thresholding of the intensity projection. (D) estimation of the sarcomere length based on ROI analysis (gray histogram, blue dashed line indicates the mean value) or RAMS analysis (red dashed line). (E)–(H), analysis corresponding to (A)–(D) for DCM (mut-int) iPSC-CM sarcomeres.

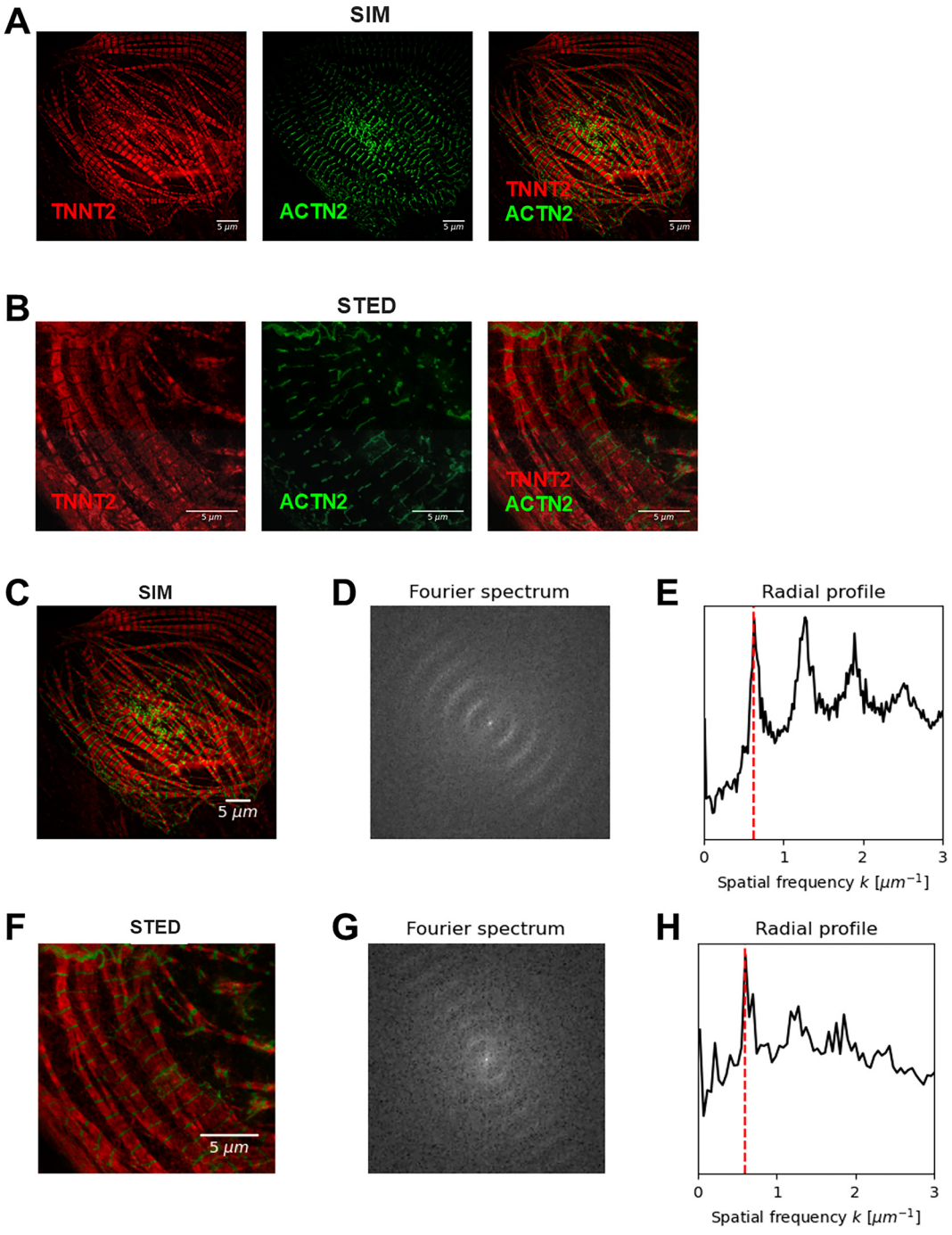


Figure 5: RAMS-based analysis of different high-resolution microscopy imaging data. (A) Structured illumination microscopy (SIM) and (B) stimulated emission depletion (STED) microscopy images of DCM (patient-specific) iPSC-CMs previously subjected to immunostaining for cardiac troponin T (TNNT2, TnT, uniprot: Troponin T), and sarcomeric alpha-actinin (ACTN2, SAA, uniprot: Alpha-actinin-2) as described in Figure 3. (C) SIM and (F) STED images were used to compute magnitude spectra (D, G). (E, H) analysis of radially averaged magnitude spectra. Red dashed line, dominant frequency or wavelength for the respective imaging data.

cardiomyocyte biomechanics as well as in translational cardiac biology investigating severe cardiac diseases such as DCM.

4 Materials and methods

4.1 Generation, culture, and cardiac differentiation of human iPSCs

All protocols for studies with human iPSC were approved by the Goettingen University Ethical Board (15/2/20 and 20/9/16An) and the Odense University Ethical Board (Projekt ID S-20140073HLP). Informed consent was obtained from all participants and all research was performed in accordance with relevant guidelines and regulations. WT iPSCs were derived and characterized as described before (Dai et al. 2023). DCM iPSCs carrying the DCM mutation tropomyosin (TPM1) L185F were generated from the isogenic WT iPSCs by CRISPR/Cas9 gene editing (DCM mutation-introduced or mut-int), or from a DCM patient carrying the inherited DCM mutation TPM1-L185F (DCM patient-specific). The generation and characterization of these iPSC lines has been reported before in detail (Dai et al. 2023). Human iPSCs were cultured on Matrigel-coated plates (Corning) utilizing chemically defined E8 medium as reported previously. Human iPSCs were passaged every four days via EDTA (Life Technologies) (Chen et al. 2011, Ebert et al. 2014), and the culture medium was changed daily. A small molecule-based approach was used to generate beating cardiomyocytes from human iPSCs, as reported previously (Dai et al. 2020, Ebert et al. 2019, Lian et al. 2012, Lian et al. 2015, Malkovskiy et al. 2021). The resulting human iPSC-CMs were subsequently cultured in RPMI (Life Technologies) with B27 supplement (Life Technologies). On day 20–25 of cardiac differentiation, the beating iPSC-CMs were dissociated using trypleE (Life Technologies), and used for experiments.

4.2 Immunostaining and confocal imaging

The human iPSC-CMs were plated on coverslips and allowed to recover for 2–3 days. Cells were fixed in 4 % paraformaldehyde and stained with primary antibodies against cardiac troponin T (TNNT2, TnT, Uniprot: troponin T, rabbit; Thermo Fisher Scientific) and sarcomeric alpha-actinin (ACTIN2, SAA, Uniprot. alpha-actinin-2, mouse, Sigma-Aldrich) overnight. Anti-Mouse IgG1 Alexa Fluor 488 and anti-Rabbit IgG (H+L; heavy light chain) Alexa Fluor 568 were used as secondary antibodies to stain coverslips. Coverslips were mounted onto glass slides and imaging was performed using a confocal microscope (LSM 710 Meta, Zeiss) equipped with a 63× oil-immersed objective, as described previously (Dai et al. 2020, Malkovskiy et al. 2021, Xu et al. 2021).

4.3 Sarcomere length analysis

ROI-based image analysis was performed by ImageJ according to previously described methods (Dai et al. 2020, Malkovskiy et al. 2021, Xu et al. 2021). From the line segments, projected intensity profiles were computed with an in-house Python routine. Peaks in the 1D real-space profiles were detected and located with Otsu thresholding as offered by Sci-kit image and connected-component labeling. Analysis via the radially averaged magnitude spectrum (RAMS) method was performed on images of the sarcomere z-disc-localized protein SAA (ACTN2) which were subjected to Fourier analysis. Based on the magnitude spectra, radial profiles in frequency space were generated and the dominant frequency was derived from the peak location. The analysis was implemented and performed in Python version 3.12 and built on the Python packages NumPy, SciPy, Scikit-image and Matplotlib.

4.4 Stimulated emission depletion microscopy (STED)

Human iPSC-CMs were plated on coverslips between day 22–26 of cardiac differentiation. Following fixation, permeabilization, and blocking, and primary antibody staining as described above, secondary antibodies (goat anti-rabbit STAR635P, ST635P-1002-500UG, Abberior, and goat anti-mouse STAR580, ST580-1001-500UG, Abberior) were applied. Finally, coverslips were mounted in ProLong Gold Antifade Mountant (Thermo Fisher Scientific). Confocal and STED images were acquired using a Leica TCS SP8 system with a HC PL APO C2S 100*x*/1.40 oil objective. Dual color STED was performed according to the spectral properties of fluorophores STAR 580 and STAR 635 P, with excitation at 580 nm and 635 nm wavelength by a white-light laser and detection between 590-625 nm and 646–699 nm, respectively. Scanning was performed at 20 nm x20nm pixel size, pixel dwell time 480 ns, scanning speed 600 Hz, 12to 16-fold line accumulation, and STED depletion at 775 nm. Raw images were processed in Fiji ImageJ.

4.5 Structured illumination microscopy (SIM)

Human iPSC-CMs were harvested between day 22–26 of cardiac differentiation and plated on coverslips, followed by fixation and immunostaining as above. 2D-SIM data were recorded using a MI-SIM (CSR Biotech Co., Ltd. (Guangzhou, China) microscope equipped with a 100*x*/1.5NA oil objective (UPLAPO100XOHR) and an ORCA-Fusion BT (Hamamatsu) sCMOS camera essentially as described previously (*27*). Images were acquired in the 2D-SIM-3 mode. Raw data were processed by Wiener reconstruction followed by sparse deconvolution (*28*).

Acknowledgments: This study was supported by the Deutsche Forschungsgemeinschaft (German Research Foundation), Sonderforschungsbereich CRC1002, project A12 (A.E.) and S02 (S.E.L.); Deutsche Forschungsgemeinschaft, Grant/Award Number: RTG 2824; and under Germany's Excellence Strategy – EXC 2067/1–390729940. D.P. is supported as associated doctoral student of the RTG2824 funded by the Deutsche Forschungsgemeinschaft. D.P. is a scholarship recipient of the Goettingen Promotionskolleg fuer Medizinstudierende, funded by the Else Kroener-Fresenius-Stiftung, EKPK.04. C.C. is supported as doctoral student of the RTG2824 funded by the Deutsche Forschungsgemeinschaft. We are grateful for support by the DZHK (German Center for Cardiovascular Research), partner site Goettingen, Germany, project IDs 81X4300123, 81X1300131. We thank for funding by the Department of Cardiology and Pneumology (Clinic for Cardiology and Pneumology) at the University Medical Center, Goettingen University and support by the Central Service Unit for Cell Sorting (BD LSRFortessa X-20 2025) at the University Medical Center, Goettingen University. M. H. gratefully acknowledges funding by the Carl-Zeiss-Stiftung within the program "CZS Stiftungsprofessuren". The STED microscopy system used in this study was jointly funded by the German State of Lower Saxony and Deutsche Forschungsgemeinschaft (DFG), project no. 243124867. We thank CSR Biotech Co., Ltd. (Guangzhou, China) for granting generous access to a live-cell MI-SIM super-resolution microscope, and help with data acquisition, image reconstruction, analysis as well as discussions.

Research ethics: All protocols for studies with human iPSCs were approved by the Goettingen University Ethical Board (IDs 7/5/24, 15/2/20 and 20/9/16).

Informed consent: Not applicable.

Author contributions: The authors have accepted responsibility for the entire content of this manuscript and approved its submission. M.H., data analysis and visualization, manuscript writing; H.N.S., performed experiments; D.P., performed experiments; C.C., performed experiments; T.K., H.N.S., STED imaging; S.J., provided essential infrastructure and advise; S.L., provided essential methods and advice; A.E., project management, supervision, manuscript writing.

Use of Large Language Models, AI and Machine Learning Tools: None declared.

Conflict of interest: The authors state no conflict of interest.

Research funding: Deutsche Forschungsgemeinschaft (German Research Foundation), Sonderforschungsbereich 1,002, project A12 (A.E.) under Germany's Excellence Strategy – EXC 2067/1–390729940 (A.E.,A.J.); DZHK (German Center for Cardiovascular Research), partner site Göttingen, Germany, project IDs 81X2300194, 81X4300123, 81X1300131 (A.E.); Clinic for Cardiology and Pneumology at the University Medical Center, Göttingen University (A.E.); RTG2824 by the Deutsche Forschungsgemeinschaft (DFG) (C.C., doctoral student and D.P., associated doctoral student); Carl Zeiss Foundation within the program "CZS Stiftungsprofessuren" (M.H.).

Data availability: The raw data can be obtained on request from the corresponding author upon reasonable request.

References

Baheux Blin, M., Loreau, V., Schnorrer, F., and Mangeol, P. (2024). PatternJ: an ImageJ toolset for the automated and quantitative analysis of regular spatial patterns found in sarcomeres, axons, somites, and more. *Biol. Open* 13, https://doi.org/10.1242/bio.060548.

Chen, G., Gulbranson, D.R., Hou, Z., Bolin, J.M., Ruotti, V., Probasco, M.D., Smuga-Otto, K., Howden, S.E., Diol, N.R., Propson, N.E., et al. (2011). Chemically defined conditions for human iPSC derivation and culture. *Nat. Methods* 8: 424–429.

Chopra, A., Kutys, M.L., Zhang, K., Polacheck, W.J., Sheng, C.C., Luu, R.J., Eyckmans, J., Hinson, J.T., Seidman, J.G., Seidman, C.E., et al. (2018). Force generation via beta-cardiac myosin, titin, and α-actinin drives cardiac sarcomere assembly from cell-matrix adhesions. *Dev. Cell* 44: 87–96 e5.

Dai, Y., Amenov, A., Ignatyeva, N., Koschinski, A., Xu, H., Soong, P.L., Tiburcy, M., Linke, W.A., Zaccolo, M., Hasenfuss, G., et al. (2020). Troponin destabilization impairs sarcomere-cytoskeleton interactions in iPSC-derived cardiomyocytes from dilated cardiomyopathy patients. *Sci. Rep*. 10: 209.

Dai, Y., Ignatyeva, N., Xu, H., Wali, R., Toischer, K., Brandenburg, S., Lenz, C., Pronto, J., Fakuade, F.E., Sossalla, S., et al. (2023). An alternative mechanism of subcellular iron uptake deficiency in cardiomyocytes. *Circ. Res*. 133: e19–e46.

Douglas, C.M., Bird, J.E., Kopinke, D., and Esser, K.A. (2024). An optimized approach to study nanoscale sarcomere structure utilizing super-resolution microscopy with nanobodies. *PLoS One* 19: e0300348.

Ebert, A.D., Diecke, S., Chen, I.Y., and Wu, J.C. (2015). Reprogramming and transdifferentiation for cardiovascular development and regenerative medicine: where do we stand? *EMBO Mol. Med.* 7: 1090–1103.

Ebert, A., Joshi, A.U., Andorf, S., Dai, Y., Sampathkumar, S., Chen, H., Li, Y., Garg, P., Toischer, K., Hasenfuss, G., et al. (2019). Proteasome-dependent regulation of distinct metabolic states during long-term culture of human iPSC-derived cardiomyocytes. *Circ. Res*. 125: 90–103.

Ebert, A.D., Kodo, K., Liang, P., Wu, H., Huber, B.C., Riegler, J., Churko, J., Lee, J., De Almeida, P., Lan, F., et al. (2014). Characterization of the molecular mechanisms underlying increased ischemic damage in the aldehyde dehydrogenase 2 genetic polymorphism using a human induced pluripotent stem cell model system. *Sci. Transl. Med*. 6: 255ra130.

Eldemire, R., Mestroni, L., and Taylor, M.R.G. (2024). Genetics of dilated cardiomyopathy. *Annu. Rev. Med*. 75: 417–426.

Eschenhagen, T. and Carrier, L. (2019). Cardiomyopathy phenotypes in human-induced pluripotent stem cell-derived cardiomyocytes – a systematic review. *Pflüger's Arch.* 471: 755–768.

Hinson, J.T., Chopra, A., Nafissi, N., Polacheck, W.J., Benson, C.C., Swist, S., Gorham, J., Yang, L., Schafer, S., Sheng, C.C., et al. (2015). Heart disease. Titin mutations in iPS cells define sarcomere insufficiency as a cause of dilated cardiomyopathy. *Science* 349: 982–986.

Lan, F., Lee, A.S., Liang, P., Sanchez-Freire, V., Nguyen, P.K., Wang, L., Han, L., Yen, M., Wang, Y., Sun, N., et al. (2013). Abnormal calcium handling properties underlie familial hypertrophic cardiomyopathy pathology in patient-specific induced pluripotent stem cells. *Cell Stem Cell* 12: 101–113.

Lian, X., Bao, X., Zilberter, M., Westman, M., Fisahn, A., Hsiao, C., Hazeltine, L.B., Dunn, K.K., Kamp, T.J., and Palecek, S.P. (2015). Chemically defined, albumin-free human cardiomyocyte generation. *Nat. Methods* 12: 595–596.

Lian, X., Hsiao, C., Wilson, G., Zhu, K., Hazeltine, L.B., Azarin, S.M., Raval, K.K., Zhang, J., Kamp, T.J., and Palecek, S.P. (2012). Robust cardiomyocyte differentiation from human pluripotent stem cells via temporal modulation of canonical Wnt signaling. *Proc. Natl. Acad. Sci. U. S. A.* 109: E1848–E1857.

Malkovskiy, A.V., Ignatyeva, N., Dai, Y., Hasenfuss, G., Rajadas, J., and Ebert, A. (2021). Integrated Ca^{2+} flux and AFM force analysis in human iPSC-derived cardiomyocytes. *Biol. Chem*. 402: 113–121.

Mcnally, E.M. and Mestroni, L. (2017). Dilated cardiomyopathy: genetic determinants and mechanisms. *Circ. Res*. 121: 731–748.

Saleem, H.N., Ignatyeva, N., Stuut, C., Jakobs, S., Habeck, M., and Ebert, A. (2024). 3D computational modeling of defective early endosome distribution in human iPSC-based cardiomyopathy models. *Cells* 13, https://doi.org/10.3390/cells13110923.

Sun, N., Yazawa, M., Liu, J., Han, L., Sanchez-Freire, V., Abilez, O.J., Navarrete, E.G., Hu, S., Wang, L., Lee, A., et al. (2012). Patient-specific induced pluripotent stem cells as a model for familial dilated cardiomyopathy. *Sci. Transl. Med*. 4: 130ra47.

Toepfer, C.N., Sharma, A., Cicconet, M., Garfinkel, A.C., Mucke, M., Neyazi, M., Willcox, J.A.L., Agarwal, R., Schmid, M., Rao, J., et al. (2019). SarcTrack. *Circ. Res*. 124: 1172–1183.

Van Der Velden, J. and Stienen, G.J.M. (2019). Cardiac disorders and pathophysiology of sarcomeric proteins. *Physiol. Rev.* 99: 381–426.

Xu, H., Wali, R., Cheruiyot, C., Bodenschatz, J., Hasenfuss, G., Janshoff, A., Habeck, M., and Ebert, A. (2021). Non-negative blind deconvolution for signal processing in a CRISPR-Edited iPSC-cardiomyocyte model of dilated cardiomyopathy. *FEBS Lett.* 595: 2544–2557.

Zhao, M.T., Ye, S., Su, J., and Garg, V. (2020). Cardiomyocyte proliferation and maturation: two sides of the same coin for heart regeneration. *Front. Cell Dev. Biol*. 8: 594226.

Zhao, B., Zhang, K., Chen, C.S., and Lejeune, E. (2021). Sarc-graph: automated segmentation, tracking, and analysis of sarcomeres in hiPSC-derived cardiomyocytes. *PLoS Comput. Biol*. 17: e1009443.

Supplementary Material: This article contains supplementary material (https://doi.org/10.1515/hsz-2025-0173).